Science Fund of the Republic of Serbia

Grant Agreement No.: 7750824

Call: IDEJE

Hybrid Integrated Satellite and Terrestrial Access Network

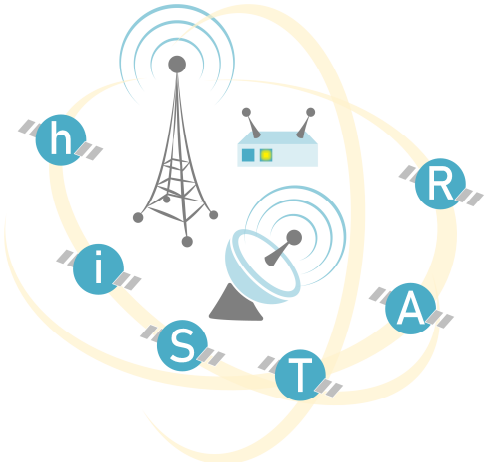

D2.1: Hybrid 5G/Sat network architecture

Work package	WP 2
Subactivity	T2.1
Due date	31/12/2022
Submission date	31/12/2022
Deliverable lead	FEE-UNIS
Version	0.8
Authors	Goran Đorđević, Srđan Brkić, Predrag Ivaniš, Vesna Blagojević
Reviewers	Dejan Drajić, Zoran Čiča

Document Revision History

Version	Date	Description of change	List of contributor(s)
V0.1	02/12/2022	1st version of D2.1	Goran Đorđević
V0.2	10/12/2022	2nd version of D2.1	Srđan Brkić
V0.3	15/12/2022	3rd version of D2.1	Predrag Ivaniš
V0.4	23/12/2022	4th version of D2.1	Vesna Blagojević
V0.5	25/12/2022	5th version of D2.1	Srđan Brkić
V0.6	28/12/2022	7th version of D2.1	Goran Đorđević
V0.7	30/12/2022	Revised version	Dejan Drajić
V0.8	31/12/2022	Revised version	Zoran Čiča

COPYRIGHT NOTICE

ACKNOWLEDGMENT

Science Fund of the Republic of Serbia

This deliverable has been written in the context of hi-STAR project who has received funding from the Science Fund of the Republic of Serbia, Programme IDEJE under grant agreement n° 7750284.

EXECUTIVE SUMMARY

The hi-STAR project addresses integration of non-terrestrial networks with terrestrial 5G network which is in focus of the next generation wireless networks. The project's main goal is to develop flexible framework for integrated terrestrial 5G and Low-Earth-Orbit (LEO) satellite networks. One of the first steps toward the framework design and implementation is defining the network architecture of the overall user access to services where user terminal has the ability to access two different RATs (Radio Access Technologies) - terrestrial and satellite.

This deliverable is a result of the work done in WP2 Subactivity T2.1 – System architecture proposal and state of the art overview. Deliverable D2.1 presents description of network architecture of the overall user access that comprises the user terminal, 5G and satellite RATs and gateway as a merge point. The selected network architecture is explained and its selection is justified. Also, for radio access parts of the architecture proper channel models and simulation environments are elaborated.

TABLE OF CONTENTS

Copyright notice 2
Acknowledgment 2
EXECUTIVE SUMMARY 3
TABLE OF CONTENTS 4
LIST OF FIGURES 5
ABBREVIATIONS 6
SECTION 1 - INTRODUCTION 7
SECTION 2 – NETWORK ARCHITECTURE ANALYSIS AND SELECTION 8
SECTION 3 – NETWORK SCENARIOS AND USE CASES 12
SECTION 4 – LEO SATELLITE LINKS 12
SECTION 5 – MILIMETER-WAVE TERRESTRIAL LINKS 28
CONCLUSIONS 20
REFERENCES 31

LIST OF FIGURES

FIGURE 1: NETWORK ARCHITECTURE OPTIONS 8
FIGURE 2: IP PACKET ENCAPSULATION 10
FIGURE 3: STEERING, SWITCHING AND SPLITTING 12
FIGURE 4: ATSSS FUNCTIONS 13
FIGURE 5: LEO CONSTELLATIONS 16
FIGURE 6: NETWORK ARCHITECTURE OF A TYPICAL LEO SYSTEM 18
FIGURE 7: DISTANCE BETWEEN HUT AND SATELLITE 19
FIGURE 8: MINIMUM AND MAXIMUM DISTANCE BETWEEN HUT AND LEO SATELLITES 19
FIGURE 9: ILLUSTRATION OF THE PROPAGATION SCENARIOS 20
FIGURE 10: SNR WAVEFORM - RESIDENTIAL USER WITH FIXED ANTENNA, RURAL AREA WITHOUT HILLS, LIGHT SHADOWING. 23
FIGURE 11: SNR WAVEFORM - HIGH-SPEED TRAIN (200 KM/H), LIGHT SHADOWING, ISOTROPIC PROPAGATION. 23
FIGURE 12: SNR WAVEFORM - MOBILE USER, SPEED OF VEHICLE IN URBAN ENVIRONMENT (40KM/H), AVERAGE SHADOWING. 24
FIGURE 13: SNR WAVEFORM - MOBILE USER WITH PEDESTRIAN SPEED, HUT IN CELL PHONE, HEAVY SHADOWING.. 24
FIGURE 14: PDF OF THE FADING ENVELOPE. 25
FIGURE 15: ACF OF THE FADING ENVELOPE. 25
FIGURE 16: ILLUSTRATION OF GAMMA-SHADOWED RICEAN FADING 26

ABBREVIATIONS

ACF	**Autocorrelation function**
ATSSS	**Access Traffic Steering, Switching and Splitting**
IP	**Internet Protocol**
ISL	**Inter-satellite links**
LEO	**Low Earth Orbit**
LOS	**Line of Sight**
MAC	**Medium-Access Control**
MP-TCP	**Multi-Path Transport Control Protocol**
PDCP	**Packet Data Convergence Protocol**
PDF	**Probability Density Function**
PL	**Physical Layer**
PoC	**Proof of Concept**
RAN	**Radio Access Network**
RAT	**Radio Access Technology**
RLC	**Radio-Link Control**
RLE	**Return Link Encapsulation**
SDAP	**Service Data Application Protocol**
SNR	**Signal-to-noise ratio**
TWDP	**Two-Wave Diffuse-Power**
WP	**Work Package**

SECTION 1 - INTRODUCTION

Deliverable D2.1 represents significant part of WP2 Subactivity 2.1 – System architecture proposal and state of the art overview. D2.1. is the first deliverable of the Subactivity 1.1 presenting work done by the end of M12 of the project. The purpose of D2.1 is to define the overall network architecture of the user's hybrid access to terrestrial 5G and satellite networks. Also, typical scenarios are analyzed which is important as these scenarios need to be part of the final PoC (Proof of Concept) that demonstrates the capabilities and benefits of the hybrid user terminal. This deliverable sets up the foundation for the definition of the user terminal system architecture and the final proof of concept demo architecture. Furthermore, proper channel models are selected and analyzed, and these models are used as the part of the simulation environment that is developed for the performance analysis.

This deliverable is structured as follows: Section 2 presents the analysis of the network architecture. The various options for the network architecture are considered, one of them is chosen for the further analysis, and the corresponding IP packet encapsulation is presented Section 3 presents the network scenarios and use cases. Low Earth orbit satellite link is considered in details in section 4, where two channel models are chosen for further analysis, and one corresponding software package is developed. Finally, in section 5 we have chosen the appropriate simulation model that will be used for the channel characterization of the millimeter-wave terrestrial links in 5G system.

SECTION 2 – NETWORK ARCHITECTURE ANALYSIS AND SELECTION

Regarding the network architecture of the overall user access that includes communication between the user terminal and the network gateway there are several possible options (Figure 1):

- Satellite RAN (Radio Access Network) is the part of the 5G ecosystem and satellite RAN is treated as 3GPP RAN [1];
- Satellite RAN is the part of the 5G ecosystem but satellite RAN is treated as non-3GPP RAN;
- Satellite and 5G RANs are treated as separate networks [2].

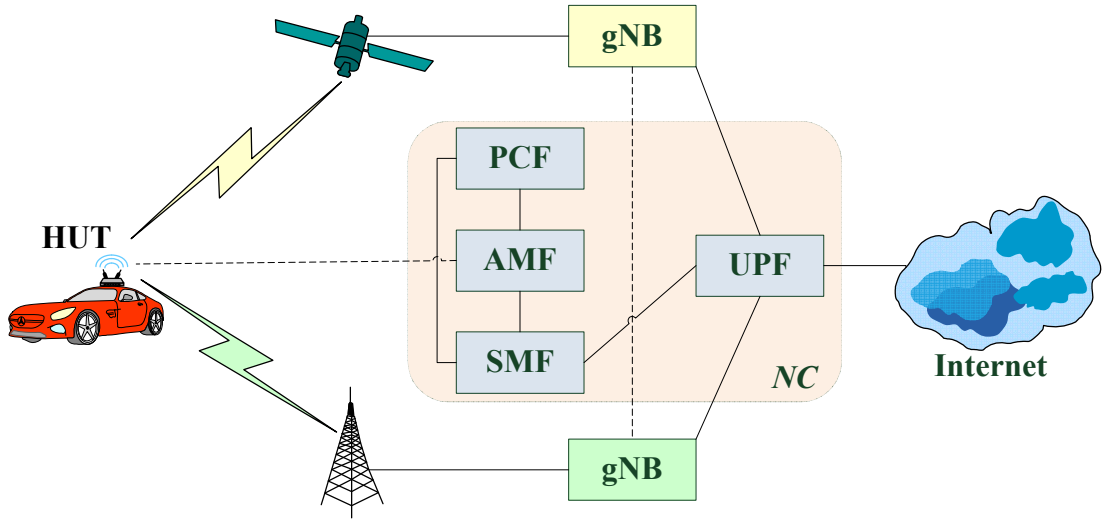

a)

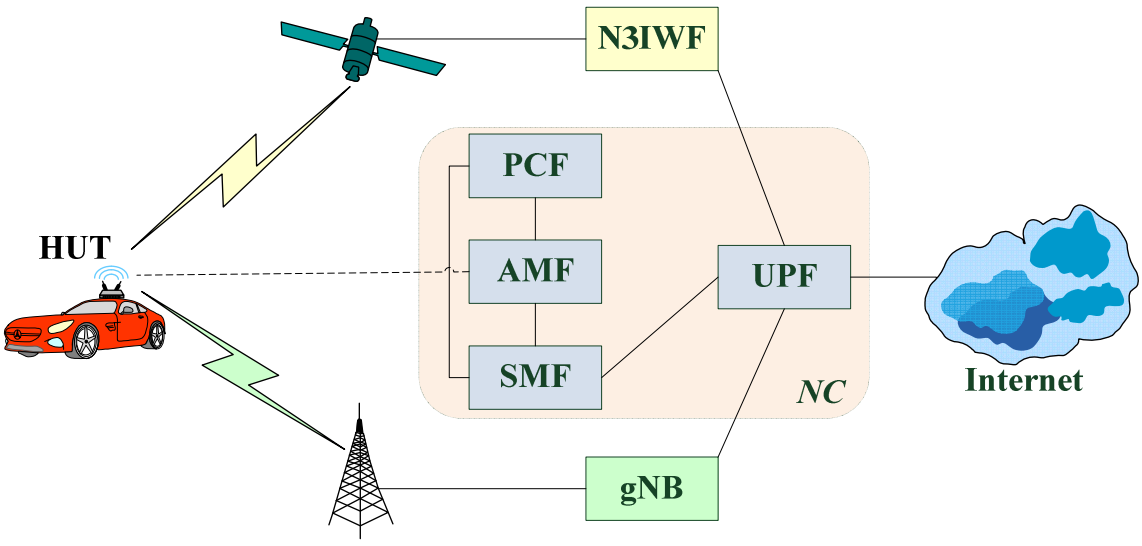

b)

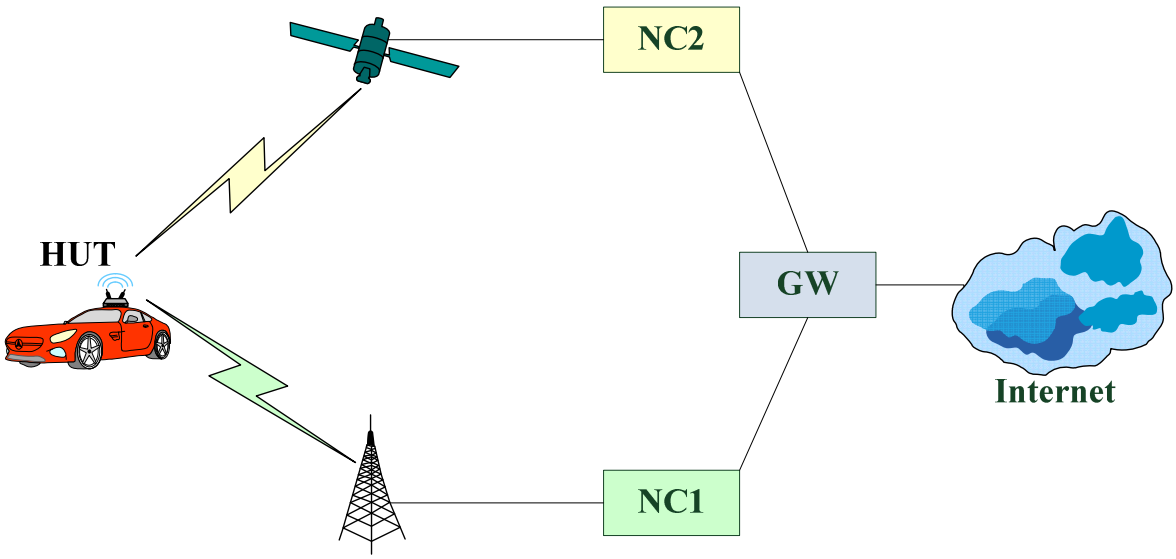

Figure 1: Network architecture options, a) Satellite RAN is the part of the 5G ecosystem and satellite RAN is treated as 3GPP RAN; b) Satellite RAN is the part of the 5G ecosystem but satellite RAN is treated as non-3GPP RAN; c) Satellite and 5G RANs are treated as separate networks.

The first two options consider that the satellite RAN is connected to 5G network core. When satellite RAN is considered as 3GPP RAN, then user accesses gNB via satellite radio link and this gNB is directly connected to network core in the same way as in terrestrial case. When satellite RAN is considered as non-3GPP RAN, then a network gateway between satellite RAN and 5G network core needs to be installed. This network gateway performs so called N3IWF (Non-3GPP Interworking Function) that is needed to adjust the non-3GPP satellite RAN to 5G core. In these two options, the provider has a better control over both RANs and can optimized traffic and traffic policies, over the RANs, more efficiently. The downside is that the both RANs must be under the control of a single service provider, which means that the satellite provider will lose the full control over the satellite RAN, and will derogate its privileges to the terrestrial operator (5G terrestrial operator). This can limit the hybrid access offers to users due to higher RAN implementation costs or the quality of the offers to users.

On the other hand, the third option considers the satellite and terrestrial networks as independent networks. In this case, there are two network cores - one satellite and one terrestrial. A network gateway is used to connect these network cores and hybrid user terminal communication is actually with this gateway via the two network cores. Mutual agreements and contracts between operators are still possible, but the overall control and optimization over the RANs are lower than in the first two options. However, this gives better chance for the operators to focus and invest only in the RAN segments of interest (terrestrial or satellite) and collaborate mutually with lower overall costs. Lastly, this option can be implemented regardless of the current state of the commercial solutions for the first two options.

In hi-STAR project, the third option will be pursued for several reasons. The first reason is that this option is readily available, unlike the other two options that are still under the development and it is yet to see in which direction the commercial solutions and operator plans will go. The second important reason is that given the availability and features of the 5G and satellite open-source solutions that are currently available, the third option is currently the only one that can be implemented in the PoC demonstration. However, the solutions and implementations that will be developed in the hi-STAR project will be able to be used in the other two options with no or minimal modifications and adjustments.

It is important to notice that IP traffic is considered to pass through the network architecture and this assumption holds for all three options of network architecture. This is a natural assumption since IP technology is dominant and used in satellite and 5G networks at network and higher protocol layers of network. Given this assumption, Figure 2 shows the IP packet encapsulation in 5G and satellite RANs.

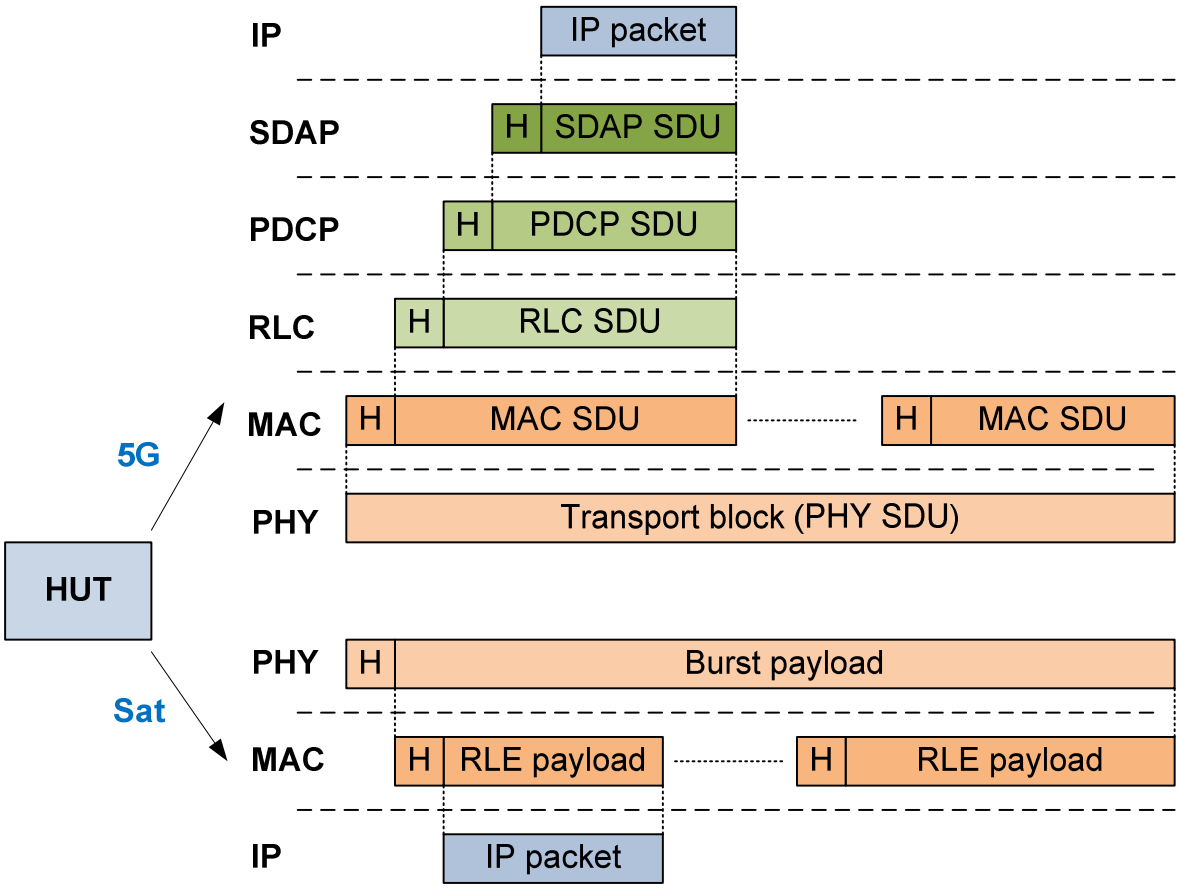

Figure 2: IP packet encapsulation

In case of 5G RAN, at user terminal IP packet passes through several layers below network layer as shown in Figure 2:

- Service Data Application Protocol (SDAP) - QoS bearers mapping to radio bearers according to their QoS requirements.
- Packet Data Convergence Protocol (PDCP) - IP header compression, ciphering, and integrity protection, retransmissions, in-sequence delivery, duplicate removal in the case of handover.
- Radio-Link Control (RLC) - segmentation and retransmission handling. RLC provides services to PDCP in form of RLC channels.
- Medium-Access Control (MAC) - multiplexing of logical channels, hybrid-ARQ retransmissions, scheduling and scheduling-related functions. The scheduling function is placed in gNB for both uplink and downlink. MAC provides services to RLC in form of logical channels.
- Physical Layer (PL) - coding/decoding, modulation/demodulation, multi-antenna mapping, and other typical physical-layer functions. Physical layer offers services to MAC layer in form of transport channels.

In case of satellite RAN, IP packet encapsulation is shown for uplink direction that is in satellite networks terminology typically denoted as return link. Communication on return link is based on time-frequency slots dedicated to each user individually. IP packets are encapsulated in RLE (Return Link Encapsulation) packets. As shown in Figure 2, depending on IP packet length, one IP packet can be split over multiple RLE packets. RLE (Return link encapsulation) packets are further encapsulated in so called the PL (Physical Layer) Bursts as shown in Figure 2.
Also, in all network architecture options there is a need for the multipath protocol that would be able to provide merging of the data flows that are split over two different RANs. This protocol can be implemented at lower and higher protocol layers. In hi-STAR we will consider higher layer implementation because our selected network architecture considers the case where RANs are independent of each other as the most general case. Thus, it is not possible to use lower layer approach because the network gateway works with network and higher protocol layers. MP-TCP (Multi-Path Transport Control Protocol) approach will be foundation of the multipath protocol that will be used in hi-STAR proposed solution.

SECTION 3 – NETWORK SCENARIOS AND USE CASES

This section presents typical network scenarios in hybrid radio access environment. These scenarios are guidelines for the hybrid user terminal features and functionalities development as well as for the PoC environment design. Also, typical use cases that would benefit from hybrid access are recognized and analyzed in terms of requirements.

Obviously, there are four possible cases regarding the state of the both RANs (terrestrial 5G and satellite):

- 5G and satellite RANs are available
- 5G RAN is available and satellite RAN is not available
- 5G RAN is not available and satellite RAN is available
- both RANs are unavailable

Of course, the last case where both RANs are not available to hybrid user terminal (HUT) is trivial in sense that user has no access to any of the networks, thus, no traffic can be sent to or received from the network. The two cases where only one RAN is available means that the all the traffic goes through the available RAN. The case where both RANs are available gives the most options to the user. In this case user can:

- load balance the traffic;
- can choose the optimal RAN for each of its services based on costs, latency, etc.;
- can use only one RAN while the other RAN serves as backup;
- can achieve greater bandwidth by using both RANs.

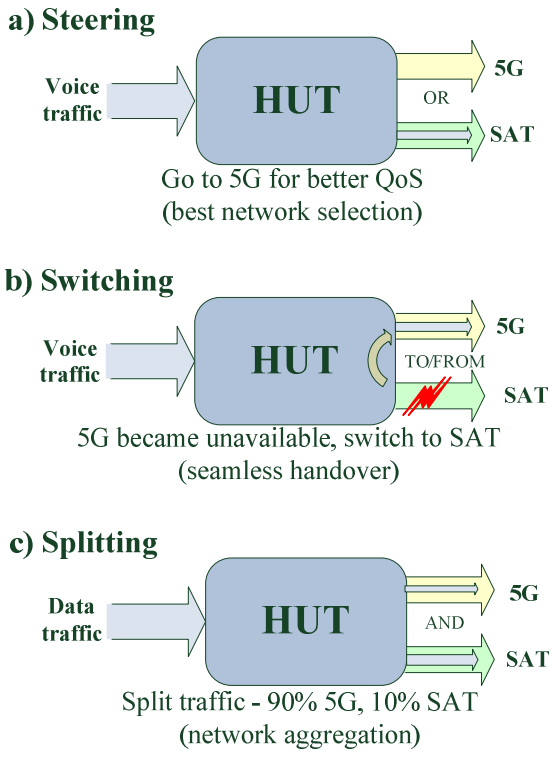

Figure 3: Steering, switching and splitting

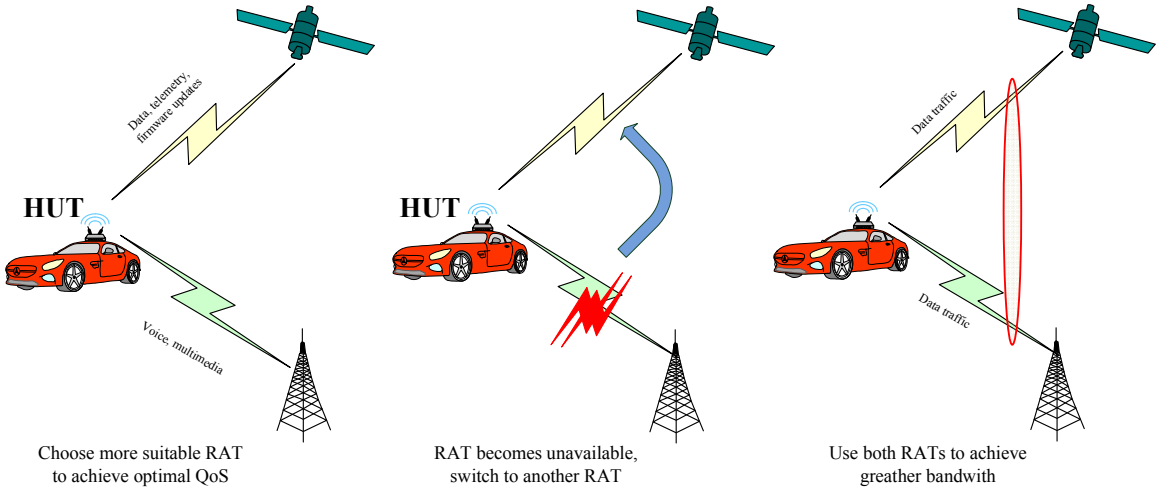

Figure 4: ATSSS functions

Actually, the traffic control in case of hybrid access is covered by the term ATSSS - Access Traffic Steering, Switching and Splitting (Figure 3). ATSSS defines three methods for traffic control. Steering means that proper RAN is selected for each of the services. This also means that complete traffic of the service goes through one RAN. Switching means handover from one RAN to another for some reason (typically loss of connection or poor link conditions). However, handover needs to maintain the continuity of the service and its traffic. Splitting considers that service uses both RANs for its traffic (typically, to increase the overall bandwidth for the service). Obviously, the hybrid user terminal needs to support ATSSS functions. The goal of the next deliverable D2.2 - HUT architecture is to propose and define the system architecture of the user terminal that will support ATSSS functions.

Hybrid access will provide most benefits to mobile user terminals that travel through various coverage zones because dual (hybrid) access will give better reliability and availability of the services. However, even the users with low mobility can feel the benefits of hybrid access in urban zones where they compete for network resources with many other users by having access to larger bandwidth via two RANs. Some of the identified services that can benefit from hybrid access are:

- telemetry with critical latency;
- telemetry with non-critical latency;
- voice and video communication (VoIP or video calls);
- cloud services;
- content access (web browsing, file downloads);
- devices updates;
- multimedia delivery.

All these services have different demands in terms of throughput, latency, jitter, etc. Given these demands, some services can prefer terrestrial RAN over the satellite RAN, which is especially the case when lower latency is required. Table 1 shows the summary of the requirements for the identified services with respect to preferred RAN, throughput and latency. Of course, this service list is not conclusive and currently it holds the initially recognized popular services. This list provides a good basis for the network scenarios described earlier in this section and for PoC demonstration.

During the hi-STAR project this list will be updated and expanded with other services as well which is the subject of WP5 subactivity 5.3 - Use cases definition and development of business models.

Table 1 - Requirements for the identified services

Use Case	Preferred RAN	Throughput	Latency
Telemetry with critical latency	5G	typically low high for high-resolution camera video	critical
Telemetry with non-critical latency	Both	low	not critical
Voice and video communication	5G	low for voice low to high for video	critical
Cloud services	Both except for latency critical services (5G)	low	typically not critical
Content access	Both	low to medium, best effort is usually used	not critical
Devices updates	Both (Satellite might provide broadcast)	low	not critical
Multimedia delivery	Both (Satellite might provide broadcast)	medium to high	not-critical expect for live event, jitter is more critical

SECTION 4 – LEO SATELLITE LINKS

Recent advances in satellite communication and launching technology renewed the interest of private companies in LEO networks. Currently there are several planned realizations of mega-constellations in low earth orbit (LEO), that are expected to make huge leap in solving the problem of digital divide by enabling Internet access all over the globe. The high throughput LEO satellites of next generation can provide complementary solution to the terrestrial networks in the segments where terrestrial infrastructure does not exist or it is not efficient, resulting in the integrated seamless satellite-terrestrial network with improved throughput, coverage and overall quality of service for the end user.

Satellites in LEO and very low Earth orbits are usually orbiting between Earth's atmosphere and inner Allen radiation belt, typically at the heights between 500 km and 1500 km above the Earth. Beside the altitude, the orbit is also determined by the orbital inclination angle, which represents the angle between the equatorial plane and the orbital plane, i.e. the plane in which the orbit lies. For a satellite orbiting the Earth directly above the Equator, the inclination angle of the orbit is □=0°. The satellites are usually grouped in orbital planes. Various orbital planes can be defined for the same inclination, as it can have different longitudes of the ascending nodes. The polar orbit represented with blue color in Fig. 5 has inclination angle θ=90°, while the green and the red orbit have the same inclination angle (θ=45°), but the different longitudes of the ascending nodes.

In general, the higher the altitude of the satellite, the larger is the footprint of the single satellite and a smaller number of satellites is needed for global coverage. Moreover, the lower altitude leads to the smaller path-loss and the propagation delay values. Satellites in LEO circular orbits have high velocity (approximately 7.7 km/s) with typical orbital periods for LEO circular orbits in the range 90-110 minutes. Due to high velocity, a satellite is visible to the user at the fixed position on the Earth only during a few minutes interval. High throughput, next generation LEO satellites of use multiple-beam antennas, so the cell covered by a beam pattern moves over the Earth's surface at a very high speed. Diameter of a single beam of the satellite at the height 1200 km is 50 km for Ku-band satellites, while they are smaller when Ka- or Q-band is used. Therefore, the user at the earth's surface is in one beam for very short interval, usually shorter than a minute. The system provides automatic switching from beam to beam within the same satellite antenna footprint, and also almost continuously perform handovers between satellites flying over the same location.

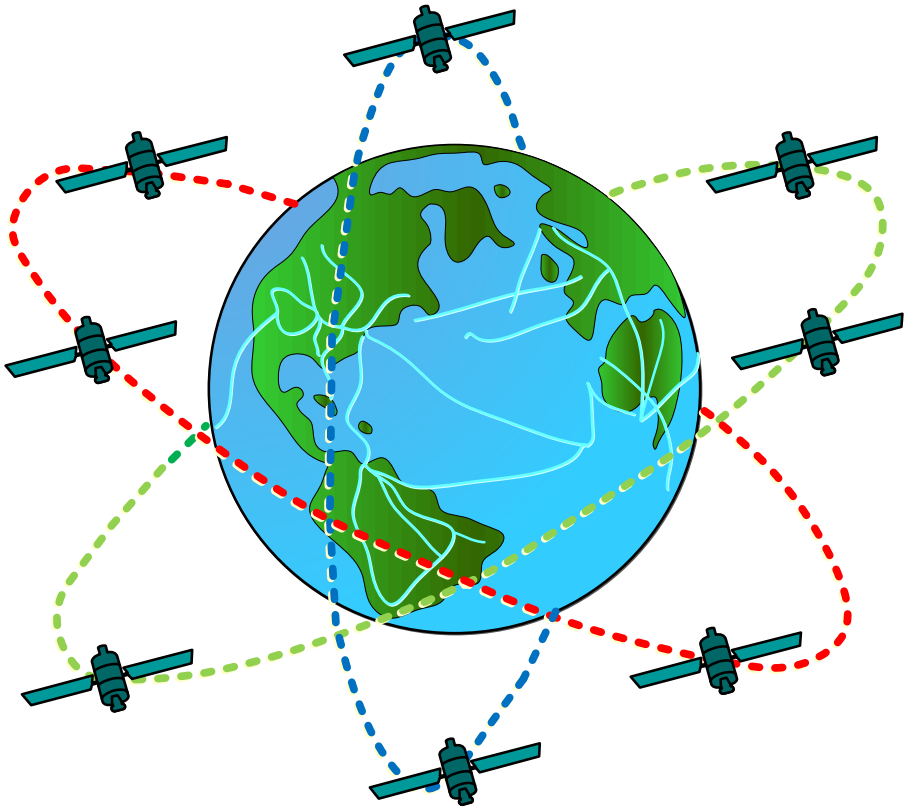

Figure 5: LEO Constellations

The first LEO satellite constellations were developed in 1990s (Iridium, Globalstar), offering communications services from space. Recently, advances in communication and launching technology renewed interest and smaller and less expensive satellites are developed. They are usually equipped with steerable multi-beam antennas and empowered with advanced signal processing capabilities. High throughputs are enabled by using spectrally efficient approaches such as frequency-reuse, higher frequency band, as well as advanced modulation and coding techniques. As a result, mega constellations with a couple of thousand, potentially tens of thousands of satellites have been proposed. Some of them are already operational (Starlink with more than 3000 launched satellites), while the others are waiting to become operational (OneWeb is expected deliver global coverage in 2023) or to be launched (Telesat, Amazon). The main purpose of these systems is to provide the high-bandwidth and low-latency internet access services across the earth.

Some details about mentioned constellations are presented in the Table 2. As an example OneWeb use 36 polar orbital planes with inclination 87.9^{o}, 32 planes with inclination 55^{o}, and 32 planes with inclination 40^{o}. The altitude is the same for all orbits, and it is equal to 1200 km. The orbit altitudes in Starlink and Amazon systems are lower, and number of satellites per one orbital plane varies between 13 and 72. Most of the systems plans to provide direct connections between neighbor satellites in the constellation by providing intra-and cross-plane free space optics inter-satellite links (ISL) with throughput greater than 20 Gb/s.

With the goal to increase the satellite utilization efficiency, the initial plan is to avoid satellite-terrestrial communication when the user terminal elevation angle is less then 10^{o}, 25^{o}, 25^{o}, and 35^{o} for Telesat, OneWeb, Starlink, and Amazon, respectively. In such a case, it is estimated that a typical mega constellation could offer a total capacity around tens of Tb/s. This throughput values would not be able to make satellite services competitive with the ones offered by current terrestrial networks (that are approximately in the range of thousands of Tb/s), but satellites could enable complementary coverage of the land infrastructure in the regions where a terrestrial infrastructure is non-existing or inappropriate [3, 4].

Table 2 – Orbit characteristics of the complete LEO constellations [3]

System	Altitude (km)	Inclination (^{o})	Planes	Satellites per plane	Number of satellites (approved)
Telesat	1015 1325	98.98 50.88	27 40	13 33	1671
OneWeb	1200 1200 1200	87.9 55 40	36 32 32	49 72 72	6372
Starlink	540 550 560 560 570	53.2 53 97.6 97.6 70	72 72 6 4 36	22 22 58 43 20	4408
Amazon	590 610 630	33 42 51.9	28 36 34	28 36 34	3236

Currently, the architecture of the typical system based on mega-constellations consists of three main components [5]:

- groups of satellites in low orbits (possibly interconnected with ISL),
- a network of ground stations (gateways),
- user terminals.

Ground stations (gateways) are positioned around the world and exchange signals with the satellites, tapping them into existing fiber-optic infrastructure. Each satellite acts as a repeater, transmitting a signal from the ground station to the user with the satellite terminal and vice versa. If inter-satellite links are not present, for successful operation, the ground station and the user must be in the field of view of the satellite at the same time. Therefore, the distance between them should not exceed approximately a thousand kilometers. However, if inter-satellite links are present, it is possible to serve users globally even when a gateway is far away (even for reduced number of gateways).

In the current plans most mega constellations use the Ka-band for feeder links (communication link between the satellite and the gateway stations) and Ku band for user communications (links that connects satellite and user). In OneWeb and Starlink, the frequency range in Ka-band are 17.8-19.3 GHz and 27.5-30.0 GHz for downlink and uplink, respectively, and the frequency range in Ku-band is 10.7-12.7 GHz and 14.0-14.5 GHz for downlink and uplink, respectively [6]. The frequency ranges in Telestar and Amazon systems are very similar.

Each satellite will have up to 32 elliptical user beams, and it will be able to form at least two steerable gateway beams. The theoretical bandwidth available to Starlink residential users, when connected with rectangular antenna of weigh 4.2 kg, is 1 Gbps. Real field measurements indicates that the average download speed of Starlink was 105 Mb/s, and the average upload speed was 12 Mb/s.

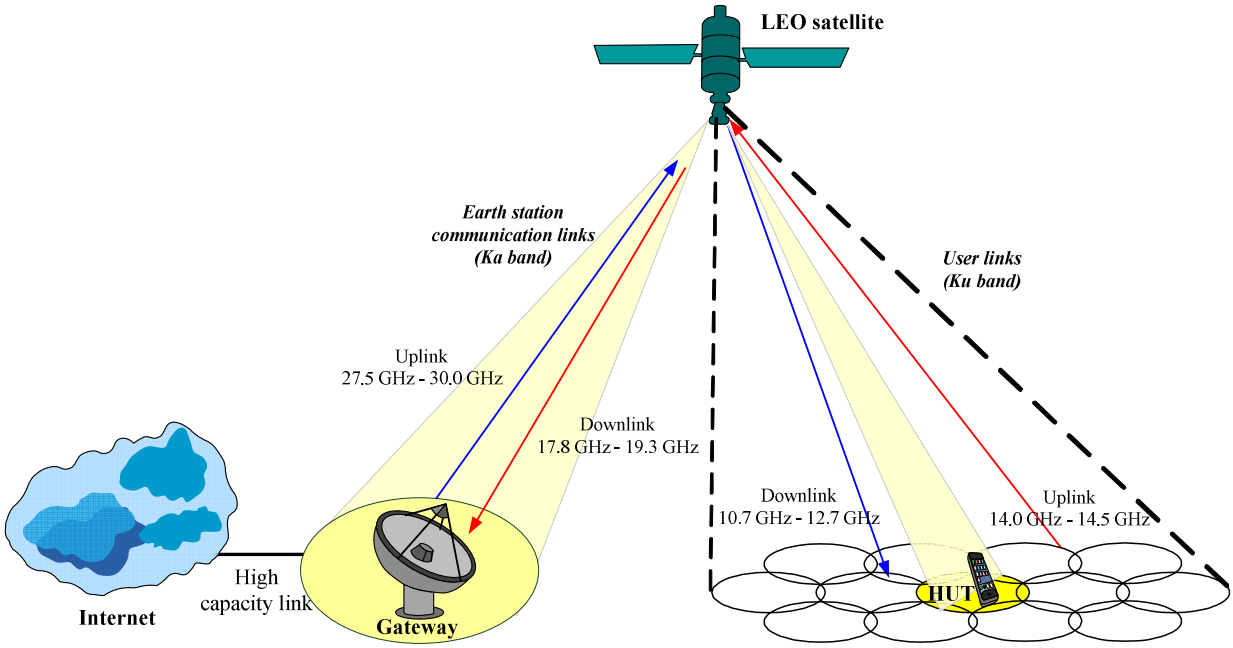

Figure 6: Network architecture of a typical LEO system

The current relative position of the HUT with respect to the satellite can be described by the altitude and the elevation angle, as illustrated in Figure 7. Since the LEO satellites are not located in fixed position, the distance between satellites and terrestrial receivers is not constant, as shown in Figure 8.

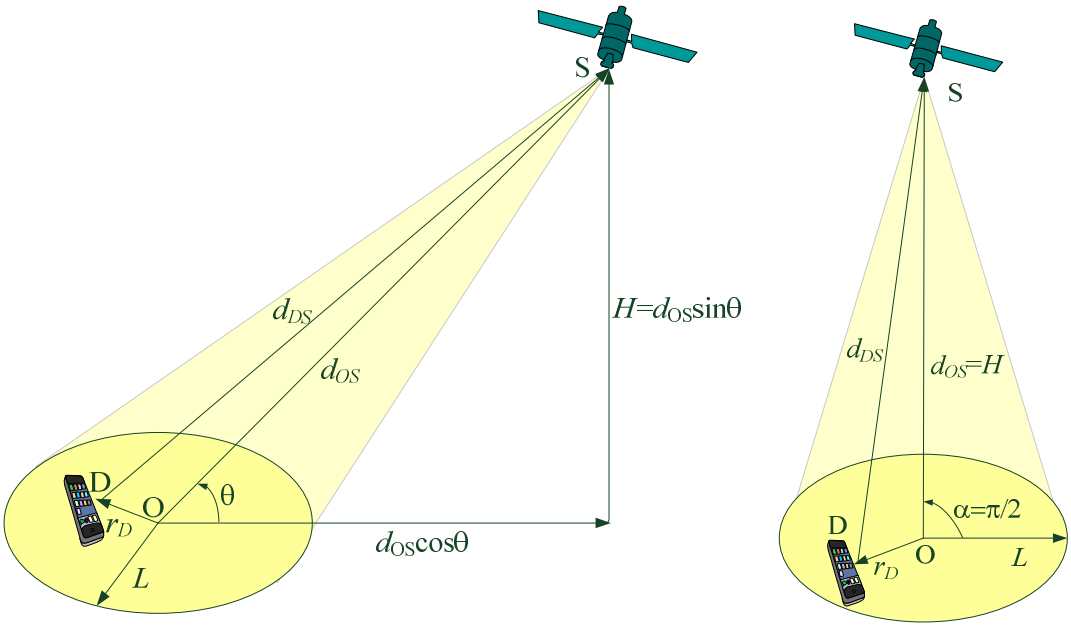

Figure 7: Distance between HUT and satellite [7]

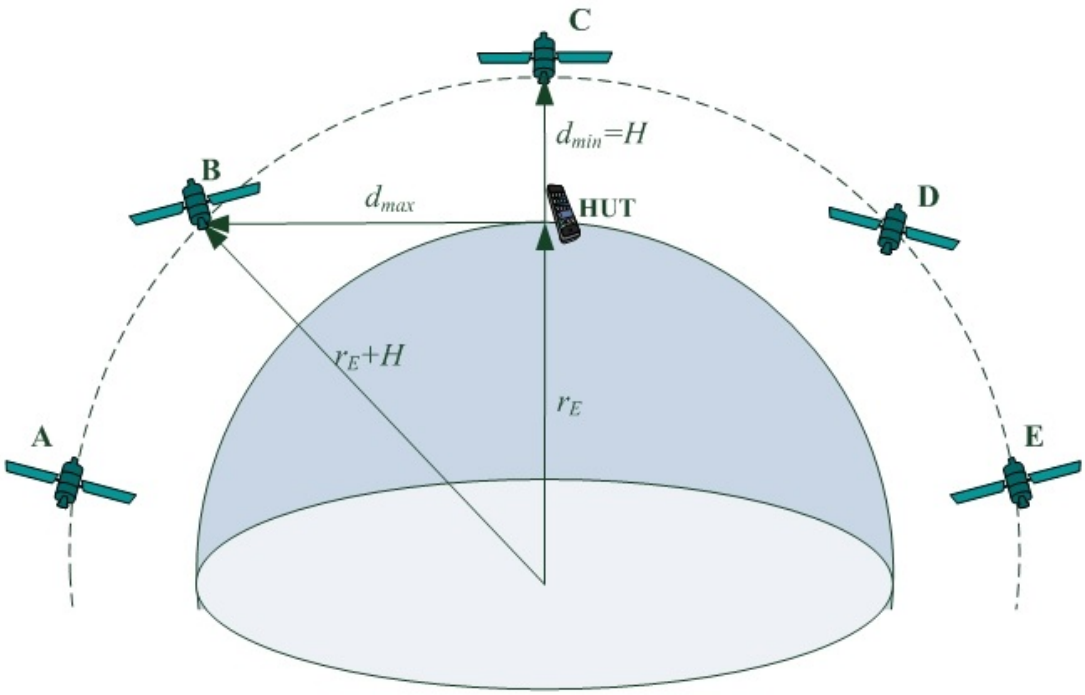

Figure 8: Minimum and maximum distance between HUT and LEO satellites [8]

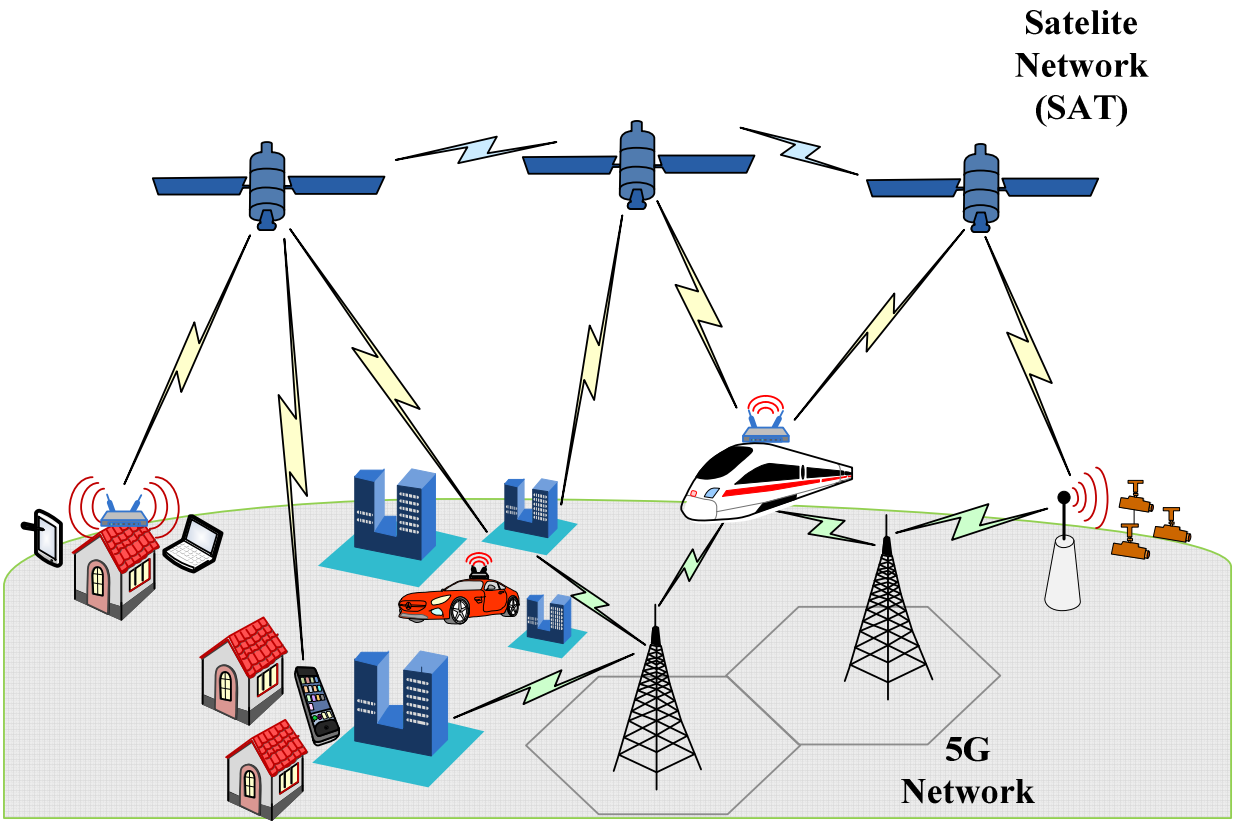

Figure 9: Illustration of the propagation scenarios

If we concentrate to the satellite segment of satellite/terrestrial network (illustrated in Figure 9), we can identify various propagation scenarios:

1. **Static or mobile HUT:** Residential user that is connected with fixed antenna and Wi-Fi are affected less by multipath fading when compared to mobile users (especially in the case when HUT is located in a high-speed train or a car).Therefore, we can consider several cases – fixed user antenna, pedestrian mobility (~5km/h), mobility in urban environment (40-50km/h), and high speed mobility (>150km/h).
2. **HUT is surrounded with buildings and hills, or it is located in urban environment:** This can result in heavy or average shadowing, as the surrounding buildings or moving objects can temporarily reduce the strength of the LOS propagation component. We can consider a few cases – light shadowing (antenna fixed in one position, or mobile user has permanent LOS connection with satellites), average shadowing (medium urban environment with outdoor mobility), and heavy shadowing (user surrounded with high concrete buildings, user is moving indoor and outdoor).
3. **Position of satellite:** The elevation angle of the satellite is known and it can affect the average received power, as well as the QoS.
4. **Position of the user:** The user is located in the centre of the beam, at the edge of the beam, or the position of the user in the beam is unknown (or the position is changed fast).

The instantaneous received signal-to-noise ratio (SNR) over the link between the transmitter and receiver on the satellite-terrestrial link can be easily obtained as

$$\gamma(t) = \frac{P_T}{\sigma^2}\frac{|h(t)|^2}{d^{\beta}},$$

where $|h(t)|^2$ is the time varying power gain on the link (that corresponds to the small scale and large scale fading), P_T is the transmit power, σ^2 is the average power of the additive white Gaussian noise, d is the distance over the link between the transmitter and the receiver, and β is the corresponding path-loss factor.

Various mathematical models are developed to describe the fluctuations of the signal envelope in a narrowband land mobile satellite channel. It is always considered that the fluctuations can be attributed to two types of fading: multipath fading (that takes into account many weak scatter components) and shadowing (refers to the random variations of the total power of the multipath components). The distributions of the components and its temporal characteristics vary in different various channel models. In Loo's model, the amplitude of the LOS component is assumed to be a lognormal random variable. Although this model almost perfectly fits with the measurement results, it the complicated expressions for the envelope probability density function (PDF) and the envelope autocorrelation function (ACF) are obtained in this case. The simplified models are usually used in mathematical analysis, and two of these models will be described in the rest of this section.

Shadowed Ricean fading model

In land mobile satellite systems, the shadowed Ricean model is widely accepted, where the complex gain can be represented as [10]

$$h(t) = a(t)e^{-\alpha(t)} + z(t)e^{j\varsigma_0}.$$

The first term corresponds to the time varying scattering component with the Rayleigh distributed amplitude $a(t)$ and uniformly distributed random phase $\alpha(t)$, and the second term corresponds to the line-of-sight (LOS) component with the Nakagami distributed amplitude $z(t)$ and deterministic phase ς_0.

If $2b_0$ denotes the average power of the scattering component, Ω the average power of the LOS component, and m denotes Nakagami parameter for LOS component, the corresponding probability density function of the envelope $r(t) = |h(t)|$ is given by

$$f_R(r) = \left(\frac{2b_0 m}{2b_0 m + \Omega}\right)^m \frac{r}{b_0} e^{-\frac{r^2}{2b_0}} {}_1F_1\left(m, 1, \frac{\Omega r^2}{2b_0(2b_0 m + \Omega)}\right), \quad r \geq 0.$$

It has been shown in paper [10] that this model fits to the measured data published in paper [9], for different channel conditions. The corresponding parameters for the light, the average, and the heavy shadowing scenarios are presented in Table 3.

Table 3 – Typical simulation parameters

Propagation scenario	b_0	m	Ω
Infrequent light shadowing	0.158	19.4	1.29
Average shadowing	0.126	10.1	0.835
Frequent heavy shadowing	0.063	0.739	0.000897

This model can be also applicable for a wide range of elevation angles, under which the satellite is observed. Based on the channel measurements given in [11] and [12], it has been shown that the parameters of the accepted model can be determined for the various elevation angles in the range $20^o \leq \theta \leq 80^o$ [10]:

$$b_0(\theta) = -4.7943\times10^{-8}\theta^3 + 5.5784\times10^{-6}\theta^2 - 2.1344\times10^{-4}\theta + 3.2710\times10^{-2}$$
$$m(\theta) = 6.3739\times10^{-5}\theta^3 + 5.8533\times10^{-4}\theta^2 - 1.5973\times10^{-1}\theta + 3.5156$$
$$\Omega(\theta) = 1.4428\times10^{-5}\theta^3 - 2.3798\times10^{-3}\theta^2 + 1.2702\times10^{-1}\theta - 1.4864$$

We have created the software package with the simulation model, as combination of Rayleigh random process and Nakagami-m random process, as defined in [10]. Rayleigh random process with arbitrary autocorrelation function is generated following the approach described in paper [13], where autoregressive model is applied. The method that transforms uncorrelated Nakagami random process into the correlated process is described in paper [14]. As the method for generating uncorrelated process with Nakagami-*m* distribution for arbitrary real valued parameter *m* can be found in [15], it can be combined with the approach from [13] and [14] to generate shadowed Ricean fading with arbitrary temporal characteristics.

Simulation results for typical system parameters, presented in Table 4, are given in next three pages. Instantaneous SNR waveforms are presented in figures 10-13 for various propagation scenarios. The waveforms in figures 10 and 11 correspond to the light shadowing both, and the corresponding PDF of the signal-to-noise ratio (or the fading envelope) is the same for these cases (figure 14). However, if the HUT is placed in high-speed-train, the multipath effect is stronger and the SNR vary faster (the difference is visible in ACF diagram, in figure 15). For the average shadowing (figure 12) and especially for the heavy shadowing (figure 13) the signal envelope is usually smaller, that can be observed from figure 14.

Table 4 – Typical simulation parameters [7]

Variable	The definition	Value
H	altitude of the LEO satellite	550 km
L	the radius of the coverage area of the LEO satellite	100 km
r_E	the radius of the Earth	6371 km
P_T	the transmit power at the LEO satellite	25 dBW
σ^2	the average power of the additive white Gaussian noise	-64 dBm
β	Path loss factor	2

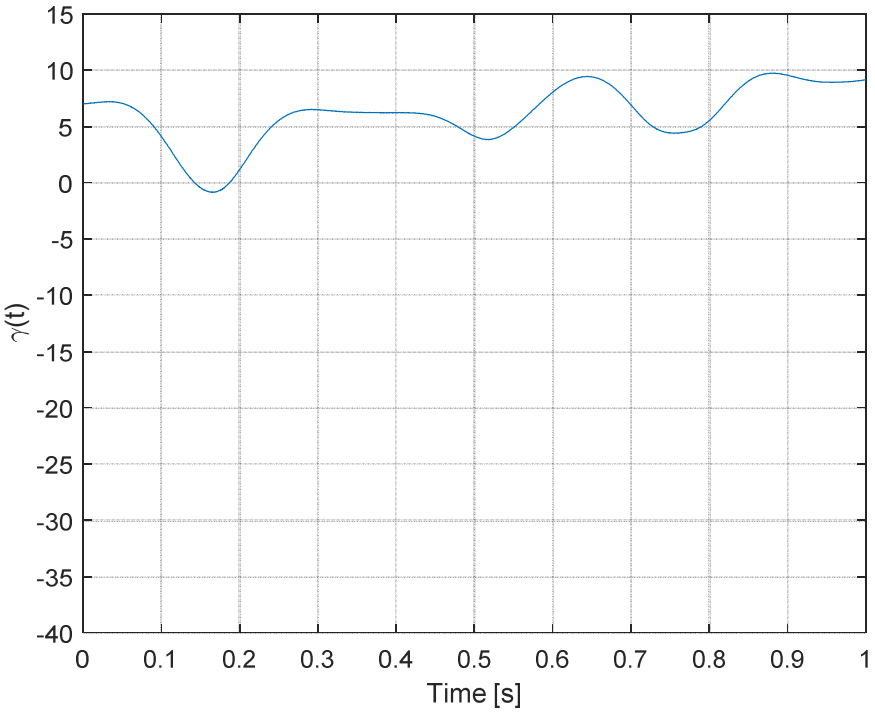

Figure 10: SNR waveform - residential user with fixed antenna, rural area without hills, light shadowing.

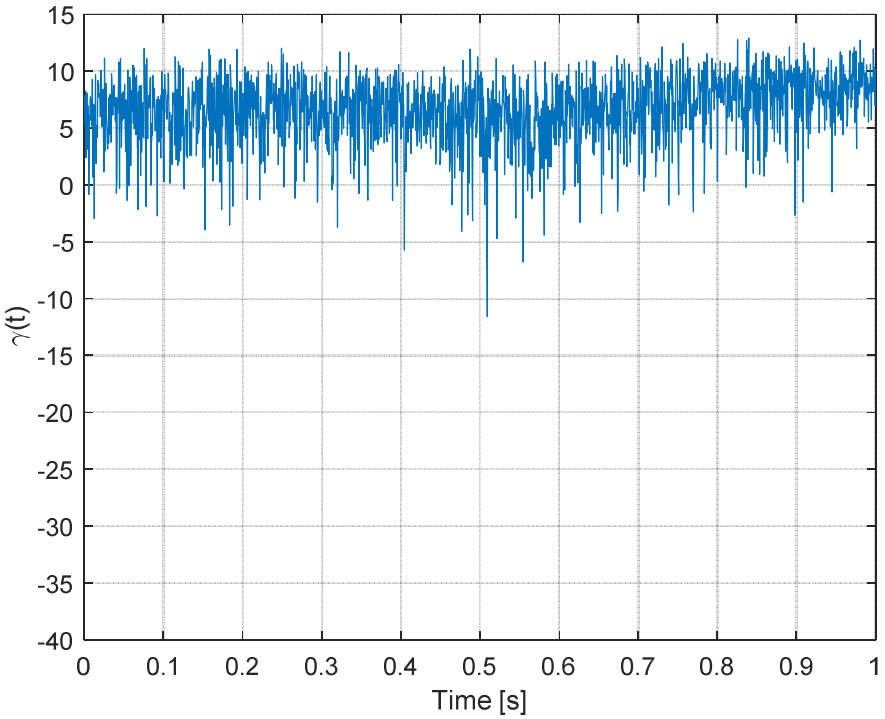

Figure 11: SNR waveform - high-speed train (200 km/h), light shadowing, and isotropic propagation.

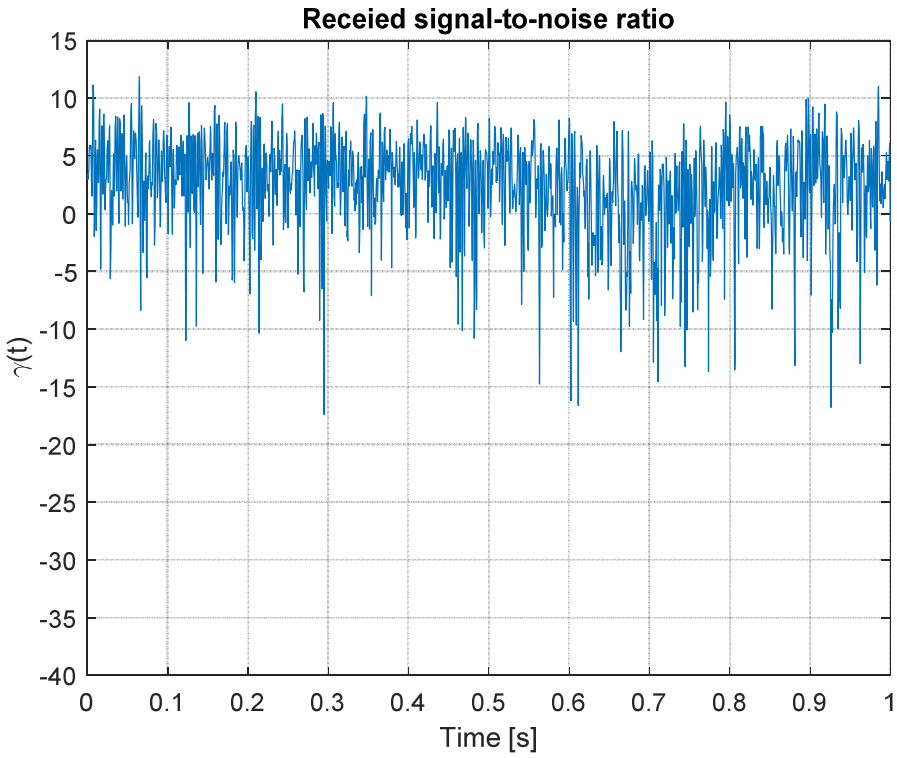

Figure 12: SNR waveform - mobile user, speed of vehicle in urban environment (40km/h), average shadowing.

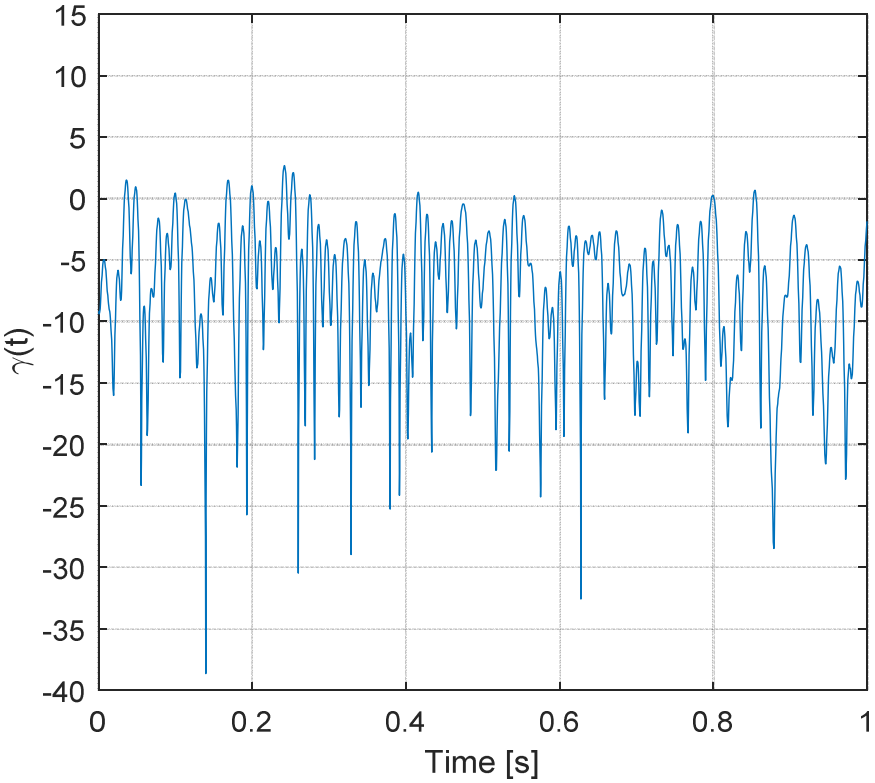

Figure 13: SNR waveform - mobile user with pedestrian speed, HUT in cell phone, heavy shadowing.

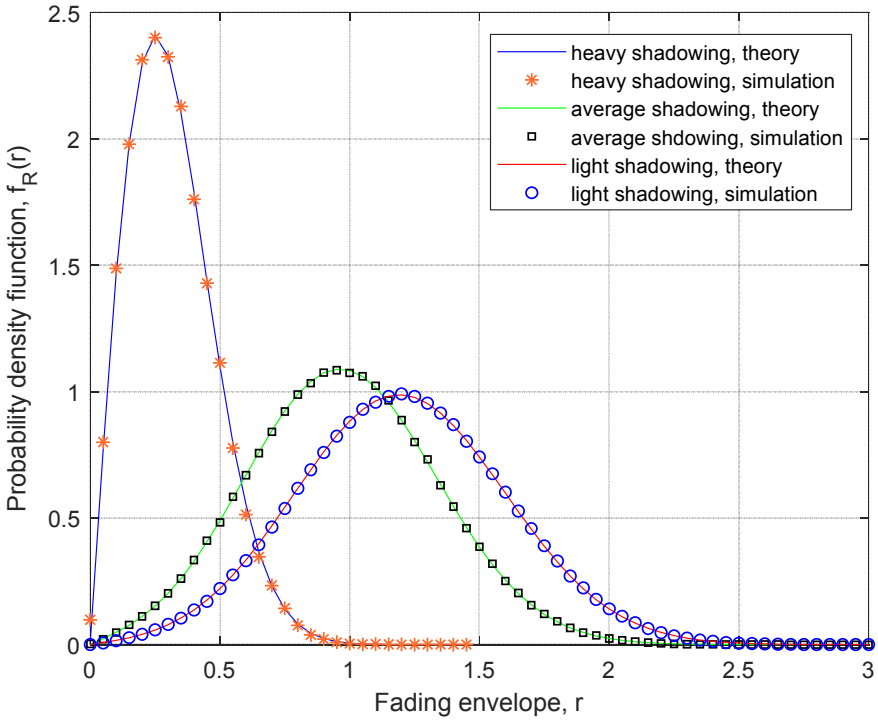

Figure 14: PDF of the fading envelope.

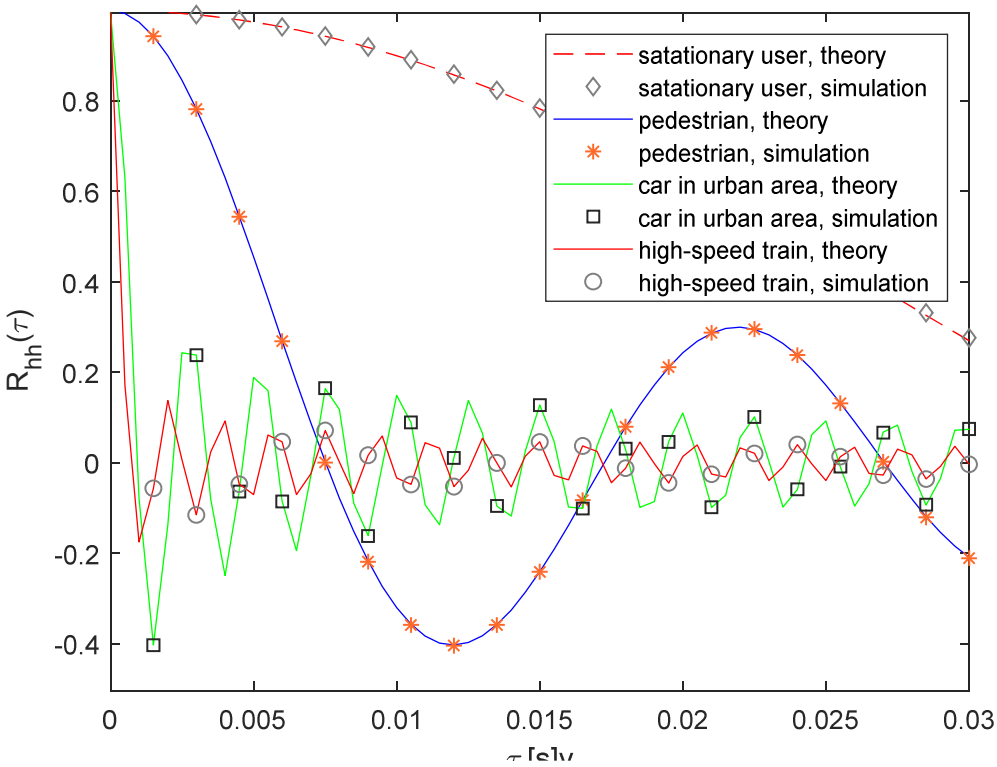

Figure 15: ACF of the fading envelope.

Gamma-shadowed Ricean fading

There are numerous statistical models that describe LMS channels [18-20], and ref therein]. In [18], the authors have listed the structures of most of the previously proposed single/mixture models [18, Table I/II]. The attributing of both multipath fading and shadowing in the random fluctuations of the propagating signal envelope is explained. Also, they innovated the shadowed Ricean model [19], assuming the line-of-sight (LOS) component as a Nakagami-*m* random variable. This model has been shown to be applicable for quite accurate numerical evaluations of satellite communication system performance.

On the other hand, the model proposed in [19-21] assumes that gamma shadowing affects simultaneously both the LOS and diffuse components. A scenario, in which both direct and scattered components are affected by the shadow effect due to the local topography of the terrain, may be characteristic in urban areas. Also, this model is general in comparison to the model which assumes that only the LOS component is shadowed.

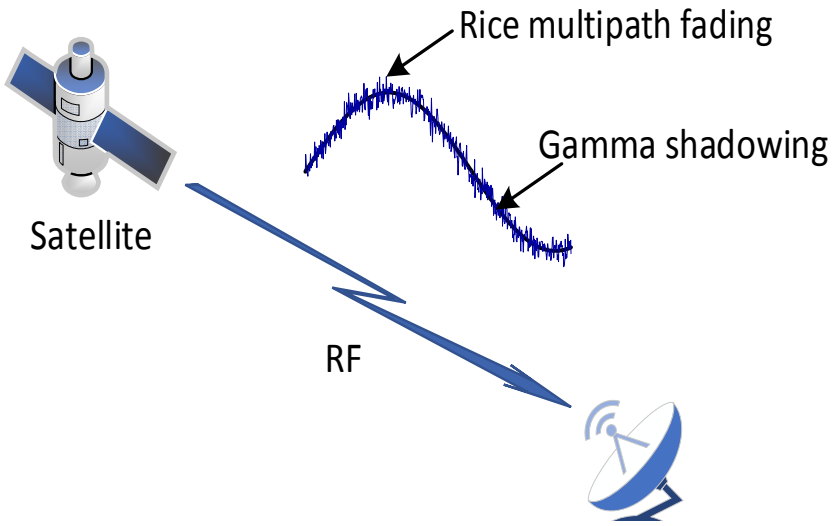

Figure 16: Illustration of Gamma-shadowed Ricean fading

Following the assumption that the channel obey gamma-shadowed Ricean fading, the PDF of the instantaneous SNR, over channel, has the following form [20, eq.(4)]

$$f_{\Gamma}(\gamma)=\frac{2e^{-K_*}}{\Gamma(m_s)}\sum_{i_*=0}^{\infty}\left(\frac{(1+K_*)m_{s_*}}{\bar{\gamma}}\right)^{\frac{m_{s*}+i_*+1}{2}}\frac{K_*^{i_*}}{(i_*!)^2}\gamma^{\frac{m_s+i_*-1}{2}}\mathrm{K}_{m_s-i_*-1}\left(2\sqrt{\frac{(1+K_*)m_s\,\gamma}{\bar{\gamma}}}\right),$$

where $\Gamma(\cdot)$ denotes the Gamma function [22, eq. (8.310)], $\mathrm{K}_{\nu}(\cdot)$ being the modified Bessel function of the second kind and the νth order [22, eq. (8.432.3)]. Parameters K_* and m_s denote the multipath fading and shadowing parameters, respectively. Usually, the K_* factor is given in dB. The parameter $\bar{\gamma}=\mathrm{E}[\gamma]$ is the average SNR.

This PDF of the instantaneous SNR over a channel is valid when both LOS and diffuse components are shadowed due to local topography in the receiver surrounding. The lower the value of parameter K_* (typical values are up to 12 dB), the multipath fading is more severe. The larger the value of parameter m_s ($0 < m_s < \infty$), the shadowing severity decreases.

After transforming the Bessel K function into Meijer's *G* function relying on and further using the argument simplification of this special function, the previous analytical form of the PDF can be rewritten as [21]

$$f_\Gamma(\gamma) = \frac{e^{-K_*}}{\Gamma(m_s)\gamma} \sum_{i=0}^{\infty} \frac{K_*^i}{(i!)^2} G_{0,2}^{2,0}\left(\frac{(1+K_*)m_s}{\bar{\gamma}} \gamma \middle| \begin{matrix} - \\ m_s, i+1 \end{matrix} \right),$$

with $G_{p,q}^{m,n}(\cdot)$ being notation for univariate Meijer's *G* function [22, eq. (9.301)], which is special built-in function in Mathematica, Maple, or Matlab software package. This channel model was used in [21].

SECTION 5 – MILIMETER-WAVE TERRESTRIAL LINKS

A general fading model is used to describe the link between the transmitting and receiving antenna, which operates in the millimeter range. According to this model, there are two specular components and a diffuse component. This fading model is known as Two-Wave Diffuse-Power (TWDP) model. This model is adequate to situation when there are two direct line-of-sight (specular) components together with a non-line-of-sight (diffuse) component over the channel. Based on the measurement verifications from [23]-[25] and the analytical models presented in [26, 27], the resulting received complex signal envelope is given by

$$V_r = V_1 e^{j\Psi_1} + V_2 e^{j\Psi_2} + x_F + jy_F$$

The resulting signal envelope consists of two specular components and a diffuse part. Specular components have constant amplitudes V_1 and V_2, and uniformly distributed phases (Ψ_1 and Ψ_2) in the interval from 0 to 2π. The diffuse component has a Rayleigh distribution. It consists of the in-phase and quadrature components (denoted by x_F and y_F) having a Gaussian distribution with zero mean value and standard deviation denoted by σ_F.

The complex fading can be presented in terms of the envelope r and argument ϑ as

$$V_r = re^{j\theta}$$

where the fading envelope is given by:

$$r = \sqrt{\left(V_1 \cos\Psi_1 + V_2 \cos\Psi_2 + x_F\right)^2 + \left(V_1 \sin\Psi_1 + V_2 \sin\Psi_2 + y_F\right)^2}\,.$$

Parametrization can be performed in two ways.

According to first way, this model of fading can be described in terms of two parameters denoted by K and Δ. The parameter K denotes the ratio of the power of the specular components to the power of the diffuse component. The parameter Δ is related to the ratio of the peak specular components power to the average specular components' power. These two parameters are defined as [26, 27]

$$K = \frac{\text{average specular power}}{\text{diffuse power}} = \frac{V_1^2 + V_2^2}{2\sigma_F^2},$$

$$\Delta = \frac{\text{peak specular power}}{\text{average specular power}} - 1 = \frac{2V_1V_2}{V_1^2 + V_2^2}\,.$$

The mean squared value of the envelope in our simulations is set to 1, i.e.

$$\overline{r^2} = V_1^2 + V_2^2 + 2\sigma^2 = 1\,.$$

On the basis of the previous equations, it follows:

$$\sigma_F = \sqrt{1/\left(2\left(K+1\right)\right)}\,.$$

Also, based on [20], it follows that:

$$V_1 = \sigma_F \sqrt{K/2}\left(\sqrt{1+\Delta} + \sqrt{1-\Delta}\right),$$

$$V_2 = \sigma_F \sqrt{K/2}\left(\sqrt{1+\Delta} - \sqrt{1-\Delta}\right).$$

When $K \to 0+$, the case correspond to the situation without specular components, i.e., the resulting PDF is the Rayleigh one. The larger the value of the parameter *K*, the larger the power of the specular components compared with the power of the diffuse component. The values of parameter Δ lie in the range from zero to one. When Δ is equal to one, the specular components have an equal amplitude, while when Δ is equal to zero, either specular component's amplitude is equal to zero.

An alternative way for parameterization was recently suggested in [26]. The authors of [26] used the same definition of parameter *K*, but instead of parameter Δ, the parameter Γ is introduced defined simply as

$$\Gamma = V_2 / V_1$$

The values of parameter Γ lie in the range from zero to one. When Γ is equal to one, specular components have equal amplitude, while when Γ is equal to zero, either specular component's amplitude is equal to zero. Without loss of generality, we assume that the mean squared value of the envelope is equal to one, i.e.,

$$\overline{r^2} = V_1^2 + V_2^2 + 2\sigma^2 = 1$$

Based on the previous expressions, it follows that

$$V_1 = \frac{K}{\left(\left(1+\Gamma^2\right)(1+K)\right)},\ V_2 = V_1 \times \Gamma$$

$$\sigma_F = \sqrt{1/\left(2(K+1)\right)}$$

On the basis of the analytical derivations presented in [29, 30], the PDF of the signal envelope can be presented as

$$f_R(r) = \frac{r}{\sigma_F^2} e^{-\frac{r^2+V_1^2+V_2^2}{2\sigma_F^2}} \left\{ I_0\left(\frac{rV_1}{\sigma_F^2}\right) I_0\left(\frac{rV_2}{\sigma_F^2}\right) I_0\left(\frac{V_1V_2}{\sigma_F^2}\right) + \right.$$

$$\left. +2\sum_{m=1}^{\infty}(-1)^m \mathrm{I}_m\left(\frac{rV_1}{\sigma_F^2}\right) \mathrm{I}_m\left(\frac{rV_2}{\sigma_F^2}\right) \mathrm{I}_m\left(\frac{V_1V_2}{\sigma_F^2}\right) \right\}$$

where $I_v(\cdot)$, $v=0,1,\cdots$ denotes a modified Bessel function of the first kind and order *v* ([22], (8.431)).

Some alternative representation of this PDF can be found in [26, 27]. However, the closed form representation does not exist.

CONCLUSIONS

This document D1.1 describes network architecture of the overall user access that comprises the hybrid user terminal, 5G and satellite RATs and gateway as a merge point. The selected network architecture is explained, and the corresponding IP encapsulation is described. The channel models adequate for analysis of satellite-terrestrial links and millimeter-wave terrestrial links are identified, and the developed simulation environments are described in details. The developed software packages, capable to create the signal waveforms that correspond to the arbitrary propagation scenarios, will be used to generate the attributes in WP4.

REFERENCES

[1] 3rd Generation Partnership Project. TR 38.821, "Solutions for NR to support non-terrestrial networks. (NTN)," V16.0.0, January 2020.

[2] ETSI TR 103 272, Satellite Earth Stations and Systems (SES); Hybrid FSS satellite/terrestrial network architecture for high speed broadband access, version 1.1.1, March 2015.

[3] N. Pachler, I. del Portillo, E. F. Crawley and B. G. Cameron, "An Updated Comparison of Four Low Earth Orbit Satellite Constellation Systems to Provide Global Broadband," *2021 IEEE International Conference on Communications Workshops (ICC Workshops)*, 2021, pp. 1-7, doi: 10.1109/ICCWorkshops50388.2021.9473799.

[4] I. del Portillo, B. G. Cameron and E. F. Crawley, "A technical comparison of three low earth orbit satellite constellation systems to provide global broadband," *Acta Astronautica*, 2019.

[5] Y. Su, Y. Liu, Y. Zhou, J. Yuan, H. Cao and J. Shi, "Broadband LEO Satellite Communications: Architectures and Key Technologies," *IEEE Wireless Communications*, vol. 26, no. 2, pp. 55-61, April 2019, doi: 10.1109/MWC.2019.1800299.

[6] Starlink analysis - forschung.fh-kaernten.at. Retrieved December 26, 2022 from https://forschung.fh-kaernten.at/roadmap-5g/files/2021/07/Starlink-Analysis.pdf

[7] G. Pan, J. Ye, J. An and S. Alouini, "Latency versus Reliability in LEO Mega-Constellations: Terrestrial, Aerial, or Space Relay," *IEEE Transactions on Mobile Computing*, doi: 10.1109/TMC.2022.3168081.

[8] H. Lin, C. Zhang, Y. Huang, R. Zhao and L. Yang, "Fine-Grained Analysis on Downlink LEO Satellite-Terrestrial mmWave Relay Networks," *IEEE Wireless Communications Letters*, vol. 10, no. 9, pp. 1871-1875, Sept. 2021, doi: 10.1109/LWC.2021.3084626.

[9] C. Loo, "A statistical model for a land mobile satellite link," *IEEE Trans. Veh. Technol.*, vol. VT–34, pp. 122–127, 1985.

[10] A. Abdi, W. C. Lau, M. -S. Alouini and M. Kaveh, "On the second-order statistics of a new simple model for land mobile satellite channels," in *Proc of IEEE 54th Vehicular Technology Conference. VTC Fall 2001.*, 2001, pp. 301-304 vol.1, doi: 10.1109/VTC.2001.956607.

[11] G. E. Corazza and F. Vatalaro, "A statistical model for land mobile satellite channels and its application to nongeostationary orbit systems," *IEEE Trans. Veh. Technol.*, vol. 43, pp. 738–742, Apr. 1994.

[12] M. Sforza and S. Buonomo, "Characterization of the LMS propagation channel at L- and S-bands: Narrowband experimental data and channel modeling," in *Proc. of NASA Propagation Experiments (NAPEX) Meeting Advanced Communications Technology Satellite (ACTS) Propagation Studies Miniworkshop*, Pasadena, CA, 1993, pp. 183–192.

[13] K. E. Baddour and N. C. Beaulieu, "Autoregressive modeling for fading channel simulation," in IEEE Transactions on Wireless Communications, vol. 4, no. 4, pp. 1650-1662, July 2005, doi: 10.1109/TWC.2005.850327.

[14] A. Papoulis and S. U. Pillai, *Probability Random Variables and Stochastic Processes*, McGraw-Hill, Boston, Mass, USA, 4th edition, 2002.

[15] J. C. Silveira Santos Filho, M. D. Yacoub and G. Fraidenraich, "A Simple Accurate Method for Generating Autocorrelated Nakagami-m Envelope Sequences," *IEEE Communications Letters*, vol. 11, no. 3, pp. 231-233, March 2007, doi: 10.1109/LCOMM.2007.061491.

[16] D. Arndt, *On Channel Modelling For Land Mobile Satellite Reception*, PhD Dissertation, der Fakultät für Elektrotechnik und Informationstechnik der Technischen Universität Ilmenau, 2014.
[17] T. Pratt, C. Bostian, J. Allnutt, *Satellite communications*, John Wiley & Sons, Second Edition, December 2019.
[18] A. Abdi, W. Lau, M.-S. Alouini, and M. Kaveh, "A new simple model for land mobile satellite channels: First and second order statistics," IEEE Trans. Wireless Commun., vol. 2, pp. 519-528, May 2003.
[19] C. Loo, "A statistical model for a land mobile satellite link," IEEE Trans. Veh. Technol., vol. VT–34, pp. 122–127, Aug. 1985.
[20] I. M. Kostic, "MGF for Gamma-Shadowed ricean fading Channel," European Trans. on Telecommun. vol. 19, pp. 155-159, Mar. 2008.
[21] J. Anastasov, P. Ivanis, G. T. Djordjevic, D. Milic, "On the Secrecy Analysis of Satellite-Terrestrial Communication Link over Gamma–shadowed Ricean Fading Channels," 2022 13th International Symposium on Communication Systems, Networks and Digital Signal Processing (CSNDSP), Porto, Portugal, July 2022. 10.1109/CSNDSP54353.2022.9908002.
[22] I.S. Gradshteyn, M. Ryzhik, *Table of Integrals, Series, and Products*, 6th ed. NewYork, NY USA: Academic, 2000.
[23] E. Zochmann, S. Caban, C. F. Mecklenbrauker, S. Pratschner, M. Lerch, S. Schwarts, M. Rupp, "Better than Rician: modelling millimeter wave channels as two-wave with diffuse power," *EURASIP Journal on Wireless Communications and Networking*, https://doi.org/10.1186/s13638-018-1336-6, pp. 1-17, 2019.
[24] T. Mavridis, L. Petrillo, J. Sarrazin, A. Benlarbi-Delai, P. De Doncker, "Near-body shadowing analysis at 60 GHz," *IEEE Transactions on Antennas and Propagation*, vol 63, no. 15, pp. 4505 – 4511, 2015.
[25] D. Kim, H. Lee, J. Kang, "Comments on "Near-body shadowing analysis at 60 GHz," *IEEE Transactions on Antennas and Propagation*, vol. 65, no. 6, pp. 3314, 2017.
[26] G. D. Durgin, T. S. Rappaport, D. A. De Wolf, "New analytical models and probability density functions for fading in wireless communications," *IEEE Transactions on Communications*, vol. 50, no. 6, pp. 1005-1015, 2002.
[27] M. Rao, F. J. Lopez-Martinez, M. S. Alouini, A. Goldsmith, "MGF approach to the analysis of generalized two-ray fading models," *IEEE Transactions on Wireless Communications*, vol. 14, no. 5, pp. 2548-2561, 2015.
[28] A. Maric, E. Kaljic, P. Njemcevic, "An Alternative Statistical Characterization of TWDP Fading Model. Sensors 2021, 21, 7513. 376 https://doi.org/10.3390/s21227513
[29] Z. Marjanović, D. N. Milić, G. T. Đorđević, "Estimation of truncation error in statistical description of communication signals over mm-wave channels," Axioms, 2022, 11(10), 569; https://doi.org/10.3390/axioms11100569 ,
[30] I. M. Kostic, "Envelope probability density function of the sum of signal, noise and interference," *Electronics Letters*, vol. 14, no. 15, pp. 490-491, 1978.